Monte Carlo study of oligopyrroles in condensed phases

Yafei Dai and Estela Blaisten-Barojas[a)]
Computational Materials Science Center and Department of Computational and Data Sciences, George Mason University, Fairfax, Virginia 22030, USA

(Received 14 December 2009; accepted 7 June 2010; published online 20 July 2010)

A classical model potential to simulate pyrrole oligomers in condensed phases is developed in this work. The new potential contains ten parameters that are optimized on a database of energy points calculated within the density functional theory approach. Based on this potential the condensed phase of systems composed of pyrrole oligomers with 4 and 12 monomers is studied as a function of system density. The binding energy, end-to-end distance, radius of gyration, vector and orientational order parameters, and pair correlation functions are reported at T=300 K. The mechanical equilibrium density is determined for both systems. The bulk modulus is reported at these densities, showing that systems composed of short oligomers are softer than systems containing longer oligomers. Analysis of pair correlation functions and order parameters indicates that at equilibrium the system of short oligomers has characteristics of a liquid while the system of longer oligomers shows a chain stacking trend. © *2010 American Institute of Physics*. [doi:10.1063/1.3457675]

I. INTRODUCTION

Polypyrrole (PPy) was discovered half a century ago[1,2] and a myriad of publications have been produced since then. PPy is a prototype conducting polymer with unique mechanical, optical, electrical, and biocompatible properties.[3] Despite the abundant literature, the physical properties and structural characteristics of pristine polypyrrole are still not well understood, and oftentimes contradictory data are found in the literature. With the advent of the new era of nanomaterials, PPy has found applications as a component at the nanoscale in a variety of sensors, fibers, and coated foams among other nanostructures.[4–6] For example, when shaped as a conduit, PPy has been proven effective for biomaterials modification and regeneration of damaged nerves.[7,8] Polymerization is achieved either electrochemically or chemically with dopant anions that remain embedded into the polymeric matrix originating the oxidized phase of PPy that possesses quinoid structure. Oxidized PPy is a polycationic conductor that synthesizes forming thin or thick films. Many electronegative dopants have been used, such as chloride ions, polystyrene sulfonate, molecular and polymeric anions, buffer salts,[9–11] and several biologically active anions[8,12] just to mention a few. By reduction, the electrical conduction property is lost and the structure of the conjugated polymer chain becomes benzenoid. The pristine polymeric PPy matrix is not crystalline, displays regions of stacked chains,[13] and is easily oxidized again by the inclusion of new dopants.[14] Electrochemical switching from oxidized to reduced phases of PPy produces up to 30% change in the sample volume. This linear actuation property is exploited for building artificial muscles.[10,15,16]

From the theoretical perspective, several *ab initio* and density functional theory (DFT) studies have investigated the structure, energetics, and electronic properties of pristine pyrrole oligomers with *n* monomers (*n*-Py) in the gas phase at various levels of theoretical depth.[17–28] However, the level of these calculations is computationally intractable for studying condensed phases that are not crystalline. For single long chain polymeric systems[29] or systems with many oligomers in the condensed phases, both Monte Carlo (MC) (Ref. 30) and molecular dynamics[31] simulations are a better choice. In classical approaches the model potential that simulates the interactions between the constituents is of paramount importance. Concerning pyrrole oligomers, there has been one group attempting the study of condensed phases of 10-Py at polymer/water interfaces and probing the effects of anion solutes on such interface.[31,32] These studies recurred to the GROMOS force field[33] parametrized for condensed phase properties of alkanes, which might not be transferable to PPy or well adapted for studies away from thermodynamic normal conditions.

In this work a new model potential of pyrrole oligomers is developed based on our previous DFT studies of *n*-Py.[27] This potential treats the Py monomers as rigid molecules with a permanent dipole moment anchored at their centers and contains interactions pertaining to intra- and interoligomer chains. Based on this potential, energetics and mechanical properties of condensed phases of pristine pyrrole oligomers are simulated as a function of density with the purpose of studying the local ordering of chains and structure in condensed phases. The paper is organized as follows. Section II describes the model potential for neutral *n*-Py. Section III presents the simulation technique based on a combination of our adaptive tempering Monte Carlo (ATMC) method[34] and standard NVT Metropolis Monte Carlo (MMC). Sections IV and V discuss the effect of density on properties of reduced 4-Py and 12-Py systems composed of 192 and 64 oligomer chains, respectively. This work is concluded in Sec. VI.

[a)]Electronic mail: blaisten@gmu.edu. URL: http://www.cmasc.gmu.edu.

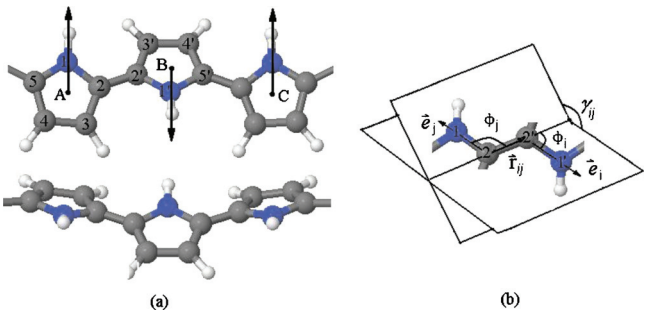

FIG. 1. Atom positions, dipoles, and angles in a PPy segment: (a) top and side views of three monomers; (b) atoms involved in the dihedral angle between two monomers.

II. MODEL POTENTIAL OF OLIGOPYRROLES

The new model potential for the reduced phase (neutral) of pyrrole oligomers containing n monomers (n-Py) treats each monomer as a rigid planar body with an electric dipole anchored at its center, as illustrated in Fig. 1(a). Depicted in this figure is a short portion of the n-Py chain with arrows indicating the position and direction of the permanent electric dipole of each monomer that is consistent with our previous DFT results.[27] The intrachain model potential U_{intra} links these monomers through various terms representing intermonomer C–C stretching, 3-monomer-bending, monomer-monomer torsion, dipole-dipole interaction, and anti-coiling with dispersive interactions. The interchain interactions U_{inter} are modeled by a 9-6 Mie–Jones function. The potential contains ten parameters with their values obtained from a numerical fit to DFT calculations[27] as it is described a few paragraphs below. Thus, for N chains of n-Py oligomers,

$$U_{\text{tot}} = \sum_{i=1}^{N} U_{\text{intra}}(i) + U_{\text{inter}}, \tag{1}$$

where for each oligomer containing n pyrrole monomers,

$$U_{\text{intra}} = U_{\text{bond}} + U_{\text{bending}} + U_{\text{torsion}} + U_{\text{dipole-dipole}} + U_{\text{anticoiling}}. \tag{2}$$

Within one oligomer, each Py monomer is considered as a rigid molecule, with its best geometry calculated from DFT,[27] and the different terms in Eq. (2) are representative of the interaction between these rigid monomers. For illustration purposes, a short oligomer segment is depicted in Fig. 1(a). Top and side views are illustrated in this figure.

Bonding between nearest-neighbor rigid monomers, U_{bond}, is represented by a Morse function linking the centers of mass of contiguous, ith and $(i+1)$th, rigid monomers at intrachain distances $r_{i,i+1}$ such that for one n-Py oligomer,

$$U_{\text{bond}} = \sum_{i=1}^{n-1} \{D_e[1 - e^{-\alpha(r_{i,i+1}-r_0)}]^2 - D_e\}, \tag{3}$$

where $r_0 = 3.8579$ Å is consistent with our previous DFT results and $D_e = 7.0196$ eV, $\alpha = 1.9197$ Å^{-1} are two parameters with values fitted to the DFT potential energy surface of bipyrrole.[27] This contribution to the potential allows for a stretching motion of any two neighboring rigid monomers along the direction of the carbon-carbon intermonomer bond within one oligomer chain.

The second term in Eq. (2) is a bending contribution, U_{bending}, that governs the angular motion between any three contiguous rigid monomers within one n-Py chain. The centers of mass of three contiguous rigid monomers are in a plane and are linked by two bonds [Eq. (3)]. Thus, the bending potential is a three-body potential that governs the angular motion between contiguous bonds by

$$U_{\text{bending}} = \sum_{i=1}^{n-2} k_\theta(\cos\,\theta_i - \cos\,\theta_0)^2, \tag{4}$$

where $\theta_0 = 139.5°$ is consistent with DFT global minimum geometries and the parameter $k_\theta = 1.2517$ eV is fitted on a series of points of the DFT potential energy surface of n-Py oligomers with n between 4 and 18.[27] For example, in the polymer portion depicted in Fig. 1(a), bending motion is possible for $\angle$ABC, which is the angle formed by joining the centers of mass A, B, C of the three depicted rigid monomers. These three contiguous rigid monomers are not coplanar and their centers of mass are not located in a straight line.

The third term in Eq. (2) is the torsion potential, U_{torsion}, describing interaction between four atoms in two contiguous rigid monomers. Motion of the pertaining dihedral angles γ between those four atoms [e.g., atoms 1, 2, 2′, 1′ in Fig. 1(b)] is described by the first two terms of the following four-body expression:

$$\begin{aligned} U_{\text{torsion}} = \sum_{i=1}^{n-1} \{ & k_1[1 - \cos(\gamma_{i,i+1} - \gamma_0)] \\ & + k_2[1 - \cos 3(\gamma_{i,i+1} - \gamma_0)] \\ & + k_3(\angle 1_i 2_i 2'_{i+1} + \angle 1_i 2_i 3_i + \angle 3_i 2_i 2'_{i+1} - 2\pi)^2\}, \end{aligned} \tag{5}$$

where $\gamma_0 = 154°$ is consistent with the DFT global minimum geometries and parameters $k_1 = 0.081$ eV, $k_2 = 0.0322$ eV, and $k_3 = 5.1808$ eV are fitted to points of the DFT potential energy surface of oligomers with several sizes.[27] The dihedral angle γ_{ij} between the ith and jth rigid monomers is

$$\cos\,\gamma_{ij} = \frac{(\vec{e}_j \times \vec{r}_{ij}) \cdot (\vec{e}_i \times \vec{r}_{ij})}{|\vec{e}_j \times \vec{r}_{ij}||\vec{e}_i \times \vec{r}_{ij}|}. \tag{6}$$

Here $\vec{e}_i$ and $\vec{e}_j$ are unit vectors contained in the planes of two contiguous rigid monomers, as shown in Fig. 1(b). The third term in Eq. (5) is a constrain that keeps atoms 1, 2, 3, and 2′ in the same plane for nearest neighboring monomers [see Fig. 1(a)]. This constrain ensures that the bond between two rigid monomers belongs simultaneously to the two planes where the monomers are defined [see Fig. 1(b)]. The constrain value is zero when the sum of the three involved angles equals 2π and is strongly repulsive otherwise.

Equation (2) contains an important dipole-dipole contribution, $U_{\text{dipole-dipole}}$, that includes the sum of all pair-interactions internal to each oligomer,

$$U_{\text{dipole-dipole}} = \sum_{i=1}^{n-1} \sum_{j=i+1}^{n} \frac{\mu^2}{r_{ij}^3} [\cos \gamma_{ij} - 3 \cos \phi_i \cos \phi_j], \quad (7)$$

where $\mu = 1.0121$ D is the magnitude of the permanent electric dipole moment of each monomer calculated with DFT,[27] γ_{ij} is the dihedral angle given in Eq. (6), and r_{ij} is the distance between point dipoles placed at the center of mass of each rigid monomer. Each dipole direction is contained in the plane of the rigid monomer and points from the center of mass toward the position of the nitrogen in that monomer, ϕ_i is the angle between the dipole $\vec{\mu}_i$ (along $\vec{e}_i$) and $\vec{r_{ij}}$, ϕ_j is the angle between $\vec{\mu}_j$ (along $\vec{e}_j$) and $\vec{r_{ij}}$ [see Fig. 1(b)]. This term in the model potential ensures a specific anisotropy of the chains that could not be captured otherwise.

The last term in Eq. (2) is a 9-6 Mie–Jones function to take into account the shape of the rigid monomers, their bent preference [Eq. (4)], and hysteric effects within a chain. In order to capture the very smooth curvature that these oligomers acquire[27] and discourage unfavorable coiling conformations, this term contains soft repulsive and dispersive interactions between second-neighbor and further-away neighbors, such that

$$U_{\text{anticoiling}} = \sum_{i=1}^{n-2} \sum_{j=i+2}^{n} 2\varepsilon \left[\left(\frac{\sigma}{r_{ij}} \right)^9 - \frac{3}{2} \left(\frac{\sigma}{r_{ij}} \right)^6 \right], \quad (8)$$

where r_{ij} are distances between the centers of mass of two noncontiguous rigid monomers within one oligomer chain and $\epsilon = 0.0069$ eV, $\sigma = 9.6801$ Å are two parameters fitted on the DFT potential energy surface of n-Py ($n = 4$, 6, 8, 12, 18). This contribution to the model potential gives a small repulsive local energy around each monomer that is enhanced if the second-neighbor bends too much. The local repulsion is larger in short oligomers than in longer chains because the negative dispersive terms compensate more when there are many further-away neighbors. Thus, this term and the bending term of Eq. (4) are to be considered together and the parameters of these two terms were fitted simultaneously as mentioned below.

The overall interaction between different oligomers n-Py and n'-Py of Eq. (2), U_{inter}, is given by

$$U_{\text{inter}} = 2\varepsilon_{\text{inter}} \sum_{i=1}^{Nn} \sum_{j=1}^{Nn'} \left[\left(\frac{\sigma_{\text{inter}}}{R_{ij}} \right)^9 - \frac{3}{2} \left(\frac{\sigma_{\text{inter}}}{R_{ij}} \right)^6 \right] + \sum_{i=1}^{Nn} \sum_{j=1}^{Nn'} \frac{\mu^2}{R_{ij}^3} [\cos \gamma_{ij} - 3 \cos \phi_i \cos \phi_j], \quad (9)$$

where R_{ij} are distances between the centers of mass of rigid monomers in two different oligomers and $\varepsilon_{\text{inter}} = 0.066$ eV, $\sigma_{\text{inter}} = 5.8686$ Å are parameters. Under this type of interaction each Py monomer is seen by another Py monomer in a different oligomer as an "effective-sphere" of core radius $(2/3)^{1/3}\sigma_{\text{inter}}$ (5.1057 Å) with a permanent dipole anchored at its center. The minimum interaction energy between two effective-spheres in two chains is $-\epsilon_{\text{intra}}$, achieved when the spheres are σ_{inter} apart. A schematic illustration of two stacked 4-Py chains is given in Fig. 2. The exponent 9 in the repulsive term is better suited for eventual penetration of neighboring effective-spheres simulating the Py monomers. Softer spheres than the usual R^{-12} of the Weeks–Chandler–Andersen[35] approach are necessary for allowing more realistic interactions between bent oligomer chains. Values of the two parameters, $\varepsilon_{\text{inter}}$ and σ_{inter}, are the optimal from a fit to a series of target points of the energy surface calculated with DFT in which one 4-Py chain is kept fixed while a second 4-Py chain is coaligned parallel to the first and rotated around at different radii in cylindrical fashion. The value of the effective-sphere core radius is slightly larger than the Py molecule size of 4.72 Å calculated with DFT because of the averaging between two chains in different relative orientations. To give an idea of the energetics involved, the interchain potential energy of the stacked configuration illustrated in Fig. 2 is −0.621 eV. There are three other minima in the radial direction with energies of −0.612, −0.571, and −0.533 eV corresponding to different relative alignments of the two chains.

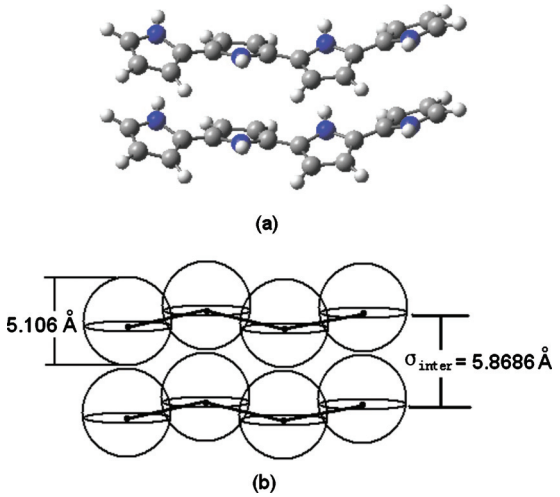

FIG. 2. Schematic representation of the way two 4-Py oligomers interact: (a) actual energetically optimized geometry of two 4-Py; (b) representation according to the excluded volume term in U_{inter} of the two chains depicted in (a).

Values of the ten parameters in Eqs. (3)–(9), D_e, α, k_θ, k_1, k_2, k_3, ϵ, σ, $\varepsilon_{\text{inter}}$, σ_{inter}, are fitted to a data set of points on the electronic energy surface of n-Py oligomers ($n = 4$, 6, 8, 12, 18) calculated with DFT.[27] The Levenberg–Marquardt algorithm (LMA) (Ref. 36) is used to optimize the fit. In this process a set of independent configurations possesses known values of the energy (target) and a set of energies from the model potential is calculated as a function of the model parameters at the same configurations of the target energies. Intrachain energies calculated with the model potential depend on eight model parameters. The LMA optimizes the parameters such that the sum of the squares of the deviations between target and model-calculated energies becomes minimal. Thus, the LMA is an iterative procedure that finds minima of the deviation-squares-sum in parameter space. According to our experience, this method has a robust performance in the optimization of models containing many parameters.[37–41] In these past studies, as well as in this work, the central component of the strategy is to have a comprehensive database of target points that contains electronic energies of representative structures.

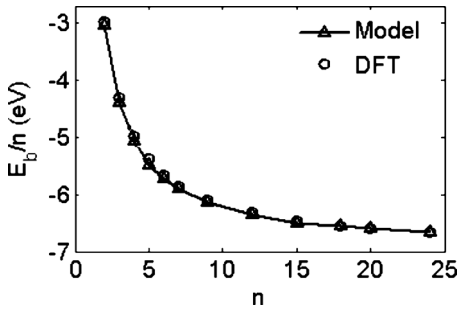

FIG. 3. Comparison of the binding energy of n-Py (n=2–7, 9, 12, 15, 18, 20, 24) calculated with the model potential and with DFT (Ref. 27).

The two parameters entering the Morse function in Eq. (3), D_e and α, are fitted on 25 target points of the electronic energy surface of 2-Py along the path that changes the C–C inter-ring bond length while keeping the torsion angle $\gamma = 154°$ and carbons 1, 2, 3, 2′ and 1′, 2′, 3′, 2 [Fig. 1(a)] maintained in the same plane. The relative error of this fit is 0.6%. Parameters k_1 and k_2 entering the torsion part of the potential in Eq. (5) are fitted on 11 target points of the electronic energy surface of 2-Py along the path that keeps the C–C inter-ring bond length fixed and changes the torsion angle γ while carbon atoms 1, 2, 3, 2′ and 1′, 2′, 3′, 2 are in the same plane. The relative error is 0.3%. The four remaining intrachain parameters k_θ, k_3, ϵ, and σ in Eqs. (4), (5), and (8) are fitted on a database of 22 target points containing the equilibrium binding energies for n-Py (n=2–9, 12, 15, 18, 24) plus ten target points from the energy surface of 4-Py. The relative error is 0.6%. The binding energy of n-Py using the model potential is further relaxed to reach a minimum of energy. These results compare very well with the target DFT values, as shown in Fig. 3. The two interchain parameters ϵ_{inter} and σ_{inter} in Eq. (9) are fitted to target points of two 4-Py and two 12-Py chains at different distances and relative orientations yielding a relative error of 1.2%.

The intrachain model potential assumes that each monomer is a rigid body. In order to locate a rigid body in space two operators $\hat{t}$ and $\hat{R}$ are needed, where $\hat{t}$ describes the translation and $\hat{R}$ describes the rotation of the rigid body. Therefore, in order to define the orientation of a rigid body in the laboratory frame e^s, the rotation matrix $\mathbb{R}$ establishes the connection to the system fixed on the rigid body e^b by $e^s = \mathbb{R}^T \cdot e^b$. The rotation matrix may be written in terms of Euler angles ϕ, ψ, θ or in terms of generalized coordinates cast in a quaternion $Q=(q_0,q_1,q_2,q_3)$.[42] The latter is adopted in this work, such that

$$\mathbb{R} = \begin{pmatrix} q_0^2+q_1^2-q_2^2-q_3^2 & 2(q_1q_2+q_0q_3) & 2(q_1q_3-q_0q_2) \\ 2(q_1q_2-q_0q_3) & q_0^2-q_1^2+q_2^2-q_3^2 & 2(q_2q_3+q_0q_1) \\ 2(q_1q_3+q_0q_2) & 2(q_2q_3-q_0q_1) & q_0^2-q_1^2-q_2^2+q_3^2 \end{pmatrix}, \tag{10}$$

where $q_0=\cos\frac{1}{2}\theta\cos\frac{1}{2}(\phi+\psi)$, $q_1=\sin\frac{1}{2}\theta\cos\frac{1}{2}(\phi-\psi)$, $q_2=\sin\frac{1}{2}\theta\sin\frac{1}{2}(\phi-\psi)$, $q_3=\cos\frac{1}{2}\theta\sin\frac{1}{2}(\phi+\psi)$, and $q_0^2+q_1^2+q_2^2+q_3^2=1$.[43] Consider $R^s(i,\nu)$ to be the position vector of the νth atom belonging to the ith monomer in the laboratory/compute system, $\vec{r}^s_{\text{CM}}(i)$ to be the position vector of its center of mass also in the laboratory/compute system, and $\vec{r}^b(\nu)$ to be the position vector of that same atom in the body system anchored in the ith monomer which is rigid. Then, atomic coordinates in the compute space are

$$\vec{r}^s(i,\nu) = \vec{r}^s_{\text{CM}}(i) + \mathbb{R}^T\vec{r}^b(\nu). \tag{11}$$

The index ν runs between 1 and 8 identifying the four carbons, three hydrogens, and one nitrogen atom in each Py monomer, except for end Py monomers where it goes up to ten due to the two extra hydrogens. The atomic positions in the body system of the rigid Py monomer are optimized in the previous DFT study.[27]

III. MONTE CARLO SIMULATION STRATEGY

With the aid of the new model potential we study systems of many 4-Py and 12-Py oligomers at densities consistent with condensed phases at T=300 K. The simulation strategy comprises two stages. In the first stage, 50 local minima of the system at low temperature are optimized with the ATMC method.[30,34] In the second stage, 50 independent NVT MMC simulations are run, each one of them starting from the results of the first stage. Properties averaged at 300 K with the MMC include potential energy, end-to-end distance, radius of gyration, order parameters, and pair correlation functions.

In the first stage, optimized configurations of the system with low energies are found via the ATMC. The ATMC is a multicanonical ensemble method that allows to find the global minimum of a system by changing the system temperature (tempering) adaptively to system location in configuration space. Systems are started at high temperatures of 1000 K, and after several thousand temperings, the algorithm drives the system to low temperatures close to zero. The simulation stops when the system reaches the state with lowest energy of all visited states and the tempering step is smaller than a prescribed accuracy. For monoatomic simple systems this minimum corresponds to the global minimum of the system. However, in the case of n-Py, there are many local minima within an energy window of 0.01 eV from the global minimum. For this reason, the ATMC is first run 50 times sequentially on each of the n-Py systems considered. The two simulation parameters of the ATMC are chosen as a=1.5 and $N_{\max}$=100. The initial configuration of the first ATMC run was a distribution of centers of mass of the chains placed inside the computational box in face-centered cubic (fcc) sites with random relative orientations and periodic boundary conditions. The 49 remaining runs were started from the optimized configuration of the previous ATMC run. Thus, after this massive tempering process, the final configuration is totally unrelated to the initial configuration used in the first run of the ATMC. In the second stage of simulations, the MMC is started from each of the 50 ATMC final low-temperature configurations. Typical MMC runs involve 500 000–1,000 000 steps for equilibration and 500 000–1 000 000 steps for the calculation of property averages.

In both ATMC and MMC, the MC step involves assigning a location in the laboratory system to all atoms in each

TABLE I. Properties of the 4-Py system at T=300 K. The equilibrium density is ρ_0=0.94 g/cm^3 and the binding energy at that density is E_{b_0}=−20.905 eV. Reported values are average ± standard deviation.

ρ (g/cm^3)	$E_b-E_{b_0}$ (eV)	$d_{\text{end-end}}$ (Å)	R_g (Å)	S	Z
0.76	0.018 ± 0.018	12.83 ± 0.01	4.02 ± 0.01	0.04 ± 0.03	0.82 ± 0.02
0.88	0.001 ± 0.018	12.83 ± 0.01	4.02 ± 0.01	0.05 ± 0.04	0.82 ± 0.03
0.94	0 ± 0.018	12.83 ± 0.01	4.02 ± 0.01	0.09 ± 0.03	0.83 ± 0.02
1.15	0.030 ± 0.018	12.82 ± 0.01	4.02 ± 0.01	0.11 ± 0.02	0.84 ± 0.03
1.35	0.140 ± 0.019	12.82 ± 0.01	4.02 ± 0.01	0.43 ± 0.03	0.84 ± 0.04
1.47	0.305 ± 0.019	12.80 ± 0.01	4.02 ± 0.01	0.77 ± 0.03	0.84 ± 0.03
1.61	0.465 ± 0.019	12.80 ± 0.01	4.01 ± 0.01	0.78 ± 0.04	0.84 ± 0.03
1.73	0.863 ± 0.019	12.78 ± 0.01	4.01 ± 0.01	0.81 ± 0.03	0.84 ± 0.02
2.00	2.038 ± 0.018	12.60 ± 0.01	3.98 ± 0.02	0.86 ± 0.02	0.85 ± 0.03

oligomer. This is accomplished in the laboratory frame by giving an initial position to each monomer center of mass, $\vec{r}^{s}_{\text{CM}}(i)_0$, and by giving an initial orientation to each monomer through its quaternion $Q(i)_0$, where $i=1,2,\ldots,n$. Then, all atoms in the oligomer chain are described in the laboratory frame using Eq. (11). With the above in mind, moving one monomer implies moving its center of mass and rotating its plane. Therefore, a new configuration obtained from the actual configuration is attained in one MC step by changing the coordinates of atoms in the ith monomer to $\vec{r}^{s}_{\text{CM}}(i)=\vec{r}^{s}_{\text{CM}}(i)+d\vec{r}$ and its orientation to $Q(i)=Q(i)+dQ$. The MC acceptance criterion is split into two parts: (a) the potential energy of the new configuration obtained by changing CM position of one monomer with dr=0.01–0.05 Å is checked for acceptance; (b) the quaternion of the selected monomer is changed by dQ=0.007–0.01 with sign from a random number in the interval [−1,1] and the new energy is tested for acceptance. Both $\vec{dr}$ and dQ change dynamically along a run in such a manner that the percentage of MMC acceptances and rejections fluctuates between 40% and 60%.

IV. CONDENSED PHASE PROPERTIES OF 4-Py SYSTEMS

The system considered here is composed of 192 chains of 4-Py oligomers. Each oligomer has 34 atoms giving a total of 6528 atoms for the full system. The purpose of these simulations is to follow the behavior of several properties of the condensed phase as a function of density at 300 K. Calculated properties at each density are obtained following the two-stage computational procedure outlined in Sec. III. Energy, radius of gyration, oligomer end-to-end distance, order parameters, and pair correlation functions are the targeted properties. This 4-Py system may be isotropically disordered, or display an ordered phase in which stacked chains become apparent at high density. A vector quasiorder parameter defined along the lines of Ref. 44 is adopted for analyzing this process identifying regions of stacked chains versus regions of fully disordered chains. A chain director axis is defined by a vector $\vec{a}=\vec{r}_1-\vec{r}_n$ joining the centers of mass of the end monomers of each n-Py oligomer. The system orientation $\vec{A}$ is defined by a vector averaging the director vectors of all chains in the system. The angle β between $\vec{a}$ and $\vec{A}$ identifies the alignment of each chain, such that the vector order parameter is

$$S=\tfrac{1}{2}\langle 3\cos^2\beta-1\rangle, \tag{12}$$

where is S=1 when β=0 or π (parallel alignment) and S=0 when $\langle\cos^2\beta\rangle=\frac{1}{3}$ (random alignment). Brackets indicate averages.

In order to describe the overall shape of each oligomer, an orientation order parameter Z (Ref. 45) is considered,

$$Z=\frac{3}{2}\left\langle\frac{1}{n}\sum_{i=1}^{n-1}\cos^2\alpha_i-\frac{1}{3}\right\rangle, \tag{13}$$

where α_i denotes the angle between the director vector of the oligomer chain and vector $\vec{r}_{i,i+1}=r_i-\vec{r}_{i+1}$ joining the ith monomer with its neighbor $(i+1)$th within each oligomer chain. A planar n-Py oligomer has Z=1 and the optimal geometry has Z=0.842.[27]

Table I summarizes results for the average values of properties calculated at T=300 K. The most stable system corresponds to a density ρ_0=0.94 g/cm^3, which is somehow lower than experiments of liquid Py reporting 0.97 g/cm^3.[46] The system equilibrium volume is V_0=90 931 Å^3. Based on

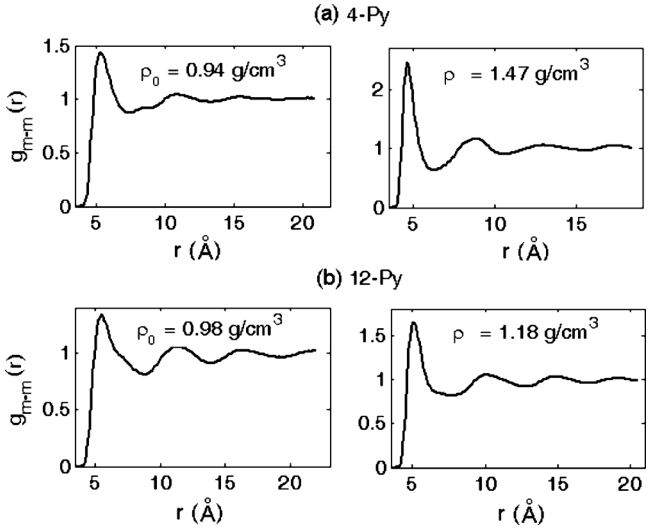

FIG. 4. Pair correlation function of interchain monomers: (a) 4-Py system; (b) 12-Py system at two densities and T=300 K.

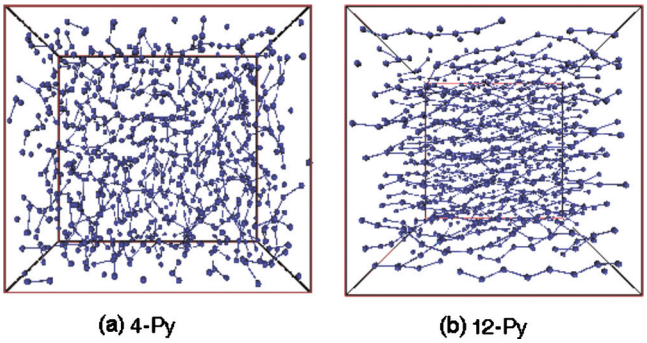

FIG. 5. Snapshot of the final simulation configurations of 4-Py and 12-Py at the corresponding equilibrium densities at T=300 K.

the change of the potential energy as a function of density, the bulk modulus $\kappa=-V(\delta^2E/\delta V^2)_T$ has a value of 118 MPa in agreement with the experimental range of 100–350 MPa of PPy films in a variety of electrolytes.[47] Based on κ, the isotropic speed of sound is 354 m/s, which is lower than speeds of around 1000 m/s measured in ordered polymeric materials. This fact emphasizes the disordered nature of our system. From the fluctuation of the energy at the equilibrium density, we estimate a vibrational contribution to the specific heat of $C_V/k_B=0.48$ at T=300 K, where k_B is the Boltzmann constant.

Figure 4(a) shows the pair correlation function between the centers of mass of all monomers calculated at the equilibrium density and at a higher density. It is clear that this oligomer system displays a local order similar to a dense fluid at the equilibrium density. As density is increased the system acquires a more definite structure. Averages of both radius of gyration and end-to-end distances are not very sensitive to density changes. Values of these properties as a function of density are given in Table I. It is expected that these two properties change little because 4-Py oligomers are energetically difficult to bend. The orientational order parameter Z is around 0.84 for all densities showing that 4-Py oligomers keep their shape at all studied densities and this shape fluctuates only slightly around the optimal geometry in the gas phase. On the other hand, the density dependence of the vector order parameter S indicates that at the equilibrium density ρ_0 the system is quite disordered. A snapshot of the final simulation configuration is given in Fig. 5(a), showing a disordered system of oligomers. However, as density increases, there is a marked transition to an ordered state apparent at densities of about 1.5 g/cm^3. Values of this order parameter are given in Table I.

V. CONDENSED PHASE PROPERTIES OF 12-Py SYSTEMS

The second system studied in this paper is composed of 64 chains of 12-Py oligomers. Each 12-Py contains 98 atoms yielding a total of 6272 atoms in the system. As in the case of shorter chains, in these simulations we study the behavior of potential energy, radius of gyration, oligomer end-to-end distance, order parameters, and pair correlation function of the condensed phase as a function of density at 300 K. Calculated properties are obtained following the two-stage ATMC/MMC computational simulation procedure outlined in Sec. III.

Table II shows the average values of properties calculated at T=300 K. The condensed phase of the 12-Py system is most stable at a density $\rho_0=0.98$ g/cm^3. Based on the change of the potential energy as a function of density, a bulk modulus $\kappa=370$ MPa is obtained. The calculated κ agrees well with the average experimental value of 300 MPa of PPy in air.[47] The sonic velocity is 614 m/s, closer to the range of speeds corresponding to ordered polymer systems. From the fluctuation of the energy at the equilibrium density, the vibrational contribution to the specific heat is estimated to be $C_V/k_B=0.54$. Averages of radius of gyration and end-to-end distances are not very sensitive to density changes. The orientational order parameter Z is around 0.77 for all densities showing that 12-Py oligomers keep their shape at the studied densities. Worth noting is that in the gas phase the Z value of 12-Py is 0.64 in its most stable configuration.[27] Therefore, in the condensed phase the 12-Py chains are flatter than in the gas phase.

Figure 4(b) shows the pair correlation function between the centers of mass of all monomers in different oligomers calculated at the equilibrium density $\rho_0=0.98$ g/cm^3 and a higher density. The 12-Py system displays local order similar to a dense fluid at the equilibrium density. At higher densities the apparent structure is more pronounced. However, as shown in Table II, the vector order parameter S increases marginally in the range of studied densities. At the equilib-

TABLE II. Properties of the 12-Py system at T=300 K. The equilibrium density is $\rho_0=0.98$ g/cm^3 and the binding energy at that density is $E_{b_0}=-76.418$ eV. Reported values are average ± standard deviation.

ρ (g/cm^3)	$E_b-E_{b_0}$ (eV)	$d_{\text{end-end}}$ (Å)	R_g (Å)	S	Z
0.66	0.141 ± 0.018	40.14 ± 0.07	12.11 ± 0.01	0.86 ± 0.03	0.77 ± 0.03
0.82	0.035 ± 0.018	40.63 ± 0.03	12.18 ± 0.01	0.94 ± 0.02	0.78 ± 0.03
0.86	0.025 ± 0.018	40.69 ± 0.05	12.19 ± 0.01	0.96 ± 0.03	0.79 ± 0.03
0.90	0.012 ± 0.018	40.66 ± 0.05	12.19 ± 0.01	0.95 ± 0.03	0.79 ± 0.02
0.96	0.003 ± 0.019	40.44 ± 0.05	12.15 ± 0.01	0.94 ± 0.03	0.79 ± 0.02
0.98	0 ± 0.019	40.32 ± 0.06	12.13 ± 0.01	0.92 ± 0.04	0.77 ± 0.03
1.05	0.022 ± 0.019	40.15 ± 0.05	12.09 ± 0.01	0.94 ± 0.03	0.77 ± 0.03
1.10	0.033 ± 0.018	40.28 ± 0.05	12.11 ± 0.01	0.95 ± 0.02	0.76 ± 0.03
1.12	0.086 ± 0.019	39.91 ± 0.04	12.06 ± 0.01	0.96 ± 0.02	0.76 ± 0.04
1.18	0.155 ± 0.019	39.74 ± 0.05	12.03 ± 0.01	0.94 ± 0.03	0.74 ± 0.05

rium density this system shows a high degree of chain ordering with small fluctuations of the vector order parameter. Figure 5(b) shows a snapshot of the last configuration, which indeed shows chain stacking.

VI. CONCLUSION

In this work we develop a new classical potential model of PPy. Using that model potential, energetics and mechanical properties of dense molecular systems of 4-Py and 12-Py containing around 6000 atoms are calculated showing good agreement of equilibrium density and bulk modulus with experiments at 300 K.[46,47] Thermal equilibrium for these condensed systems is attained by a combined simulation based on the adaptive tempering Monte Carlo method followed by standard Metropolis Monte Carlo. Findings show that the energy of the system has a minimum as a function of density, identifying the mechanical equilibrium density of 0.94 g/cm^3 for the 4-Py system and 0.98 g/cm^3 for the 12-Py system. Bulk moduli at these densities and $T=300$ K are 118 and 370 MPa, respectively. The low value of the isotropic elastic modulus indicates that systems of shorter chains are considerably softer and easier to deform than systems composed of longer chains. Pyrrole oligomer properties such as end-to-end distance and radius of gyration display only marginal changes as a function of density. The orientational order parameter Z characterizing the shape of individual molecules is almost independent of the density showing that while 4-Py oligomers keep their gas phase shape the 12-Py oligomers are considerably flatter in the condensed phase than in the gas phase. The vector quasiorder parameter S shows a marked increase as a function of density in the 4-Py, and shows that at the equilibrium density this system is fully disordered with liquidlike characteristics. On the other hand, the 12-Py system behaves quite differently showing almost perfect ordering below and above the equilibrium density. Inspection of the radial distribution functions of distances between monomers in different oligomers reveals an overall behavior characteristic of amorphous systems. The new model potential should be useful to study a variety of other properties of pristine PPy, including applications such as tissue replacement and devices where actuation is required.

ACKNOWLEDGMENTS

We acknowledge the National Science Foundation (Grant No. CHE-0626111) for partial support and the TeraGrid (Grant No. CHE100033) for the computer time allocation in the Pittsburgh Supercomputing Center.

[1] A. DallOlio, G. Dascola, V. Varraca, and V. Bocchi, Gazz. Chim. Ital. **46**, 279 (1961).
[2] G. P. Gardini, Adv. Heterocycl. Chem. **15**, 67 (1973).
[3] C. K. Chiang, C. R. Fincher, Y. W. Park, A. J. Heeger, H. Shirakawa, E. J. Louis, S. C. Gau, and A. G. MacDiarmid, Phys. Rev. Lett. **39**, 1098 (1977).
[4] J. H. Schon, A. Dodabalapur, S. Kloc, and B. Batlogg, Science **290**, 963 (2000).
[5] C. Li, H. Bai, and G. Q. Shi, Chem. Soc. Rev. **38**, 2397 (2009) and references therein.
[6] H. D. Tran, D. Li, and R. B. Kaner, Adv. Mater. (Weinheim, Ger.) **21**, 1487 (2009) and references therein.
[7] B. Garner, A. Georgevich, A. J. Hodgson, L. Liu, and G. G. J. Wallace, J. Biomed. Mater. Res. **44**, 121 (1999).
[8] J. Y. Lee, C. Bashur, A. Goldstein, and C. E. Schmidt, Biomaterials **30**, 4325 (2009) and references therein.
[9] E. Smela and N. Gadegaard, J. Phys. Chem. B **105**, 9395 (2001).
[10] E. Smela and N. Gadegaard, Adv. Mater. (Weinheim, Ger.) **15**, 481 (2003).
[11] R. E. Ansari, E-Journal of Chemistry **3**, 186 (2006).
[12] J. H. Collier, J. P. Camp, T. W. Hudson, and C. E. Schmidt, J. Biomed. Mater. Res. Part A **50**, 574 (2000).
[13] J. Fink, B. Scheerer, W. Wernet, M. Monkenbusch, G. Wegner, H.-J. Freud, and H. Gonska, Phys. Rev. B **34**, 1101 (1986).
[14] M. R. Warren and J. D. Madden, Synth. Met. **156**, 724 (2006).
[15] X. Wang, B. Shapiro, and E. Smela, Adv. Mater. (Weinheim, Ger.) **16**, 1605 (2004).
[16] J. D. Madden, N. Wandesteeg, P. Anquetil, P. Madden, A. Takshi, R. Pytel, S. Lafontaine, P. Wieringa, and I. Hunter, IEEE J. Ocean. Eng. **29**, 706 (2004).
[17] J. L. Brédas, G. B. Street, B. Thémans, and J. M. André, J. Chem. Phys. **83**, 1323 (1985).
[18] M. Kofranek, T. Kovar, A. Karpfen, and H. Lischka, J. Chem. Phys. **96**, 4464 (1992).
[19] D. Beljonne and J. L. Bredas, Phys. Rev. B **50**, 2841 (1994).
[20] R. Colle and A. Curioni, J. Am. Chem. Soc. **120**, 4832 (1998).
[21] U. Salzner, P. G. Pickup, R. A. Poirier, and J. B. Lagowski, J. Phys. Chem. A **102**, 2572 (1998).
[22] I. Rabias and B. J. Howlin, Comput. Theor. Polym. Sci. **11**, 241 (2001).
[23] B. F. G. I. Ivanov and D. Yaron, Synth. Met. **116**, 111 (2001).
[24] R. Burcl, R. D. Amos, and N. C. Handy, Chem. Phys. Lett. **355**, 8 (2002).
[25] X. Lin, J. Li, E. Smela, and S. Yip, Int. J. Quantum Chem. **102**, 980 (2005).
[26] S. Okur and U. Salzer, J. Phys. Chem. **112**, 11842 (2008).
[27] Y. Dai and E. Blaisten-Barojas, J. Chem. Phys. **129**, 164903 (2008).
[28] Y. Dai, S. Chowdhury, and E. Blaisten-Barojas, "Density functional theory study of the structure and energetics of negatively charged oligopyrroles," Int. J. Quantum Chem. (published online 29 June 2010), doi:10.1002/qua.22659.
[29] E. Blaisten-Barojas and M. Nyden, Chem. Phys. Lett. **171**, 499 (1990).
[30] X. Dong, D. Klimov, and E. Blaisten-Barojas, Mol. Simul. **33**, 577 (2007).
[31] J. J. López Cascales, A. J. Fernández, and T. F. Otero, J. Phys. Chem. B **107**, 9339 (2003).
[32] J. J. López Cascales and T. F. Otero, Macromol. Theory Simul. **14**, 40 (2005).
[33] W. F. V. Gunsteren and H. J. C. Berendsen, GROMOS: Groningen Molecular Simulation Software Package, 9747AG Groningen, The Netherlands, 1987.
[34] X. Dong and E. Blaisten-Barojas, J. Comput. Theor. Nanosci. **3**, 118 (2006).
[35] J. D. Weeks, D. Chandler, and H. C. Andersen, J. Chem. Phys. **54**, 5237 (1971).
[36] K. Levenberg, Q. Appl. Math. **2**, 164 (1944).
[37] A. Patrick, X. Dong, T. Allison, and E. Blaisten-Barojas, J. Chem. Phys. **130**, 244704 (2009).
[38] X. Dong, G. M. Wang, and E. Blaisten-Barojas, Phys. Rev. B **70**, 205409 (2004).
[39] G. M. Wang, E. Blaisten-Barojas, A. E. Roitberg, and T. P. Martin, J. Chem. Phys. **115**, 3640 (2001).
[40] C. H. Chien, E. Blaisten-Barojas, and M. R. Pederson, J. Chem. Phys. **112**, 2301 (2000).
[41] E. Blaisten-Barojas and S. N. Khanna, Phys. Rev. Lett. **61**, 1477 (1988).
[42] D. J. Evans and S. Murad, Mol. Phys. **34**, 327 (1977).
[43] M. P. Allen and D. J. Tildesley, *Computer Simulation of Liquids* (Clarendon, Oxford, 1990).
[44] P. G. D. Gennes and J. Prost, *The Physics of Liquid Crystals* (Oxford University, Oxford, 1995).
[45] Z. Usatenko and J. U. Sommer, Macromol. Theory Simul. **17**, 39 (2008).
[46] A. L. Harreus, *UIImanms Encyclopedia of Industrial Chemistry* (Wiley, Weinheim, 2002).
[47] R. Z. Pytel, E. L. Thomas, and I. W. Hunter, Polymer **49**, 2008 (2008).